Applied Physics Letters

High-contrast level-crossing resonances in a small cesium vapor cell for applications in atomic magnetometry

Cite as: Appl. Phys. Lett. **119**, 024001 (2021); https://doi.org/10.1063/5.0059019
Submitted: 04 June 2021 . Accepted: 02 July 2021 . Published Online: 13 July 2021

D. V. Brazhnikov, V. I. Vishnyakov, S. M. Ignatovich, I. S. Mesenzova, C. Andreeva, and A. N. Goncharov

Applied Physics Letters ARTICLE scitation.org/journal/apl

High-contrast level-crossing resonances in a small cesium vapor cell for applications in atomic magnetometry

Cite as: Appl. Phys. Lett. **119**, 024001 (2021); doi: 10.1063/5.0059019
Submitted: 4 June 2021 · Accepted: 2 July 2021 ·
Published Online: 13 July 2021

D. V. Brazhnikov,[1,2,a] V. I. Vishnyakov,[1] S. M. Ignatovich,[1] I. S. Mesenzova,[1] C. Andreeva,[3,4] and A. N. Goncharov[1,2,5]

AFFILIATIONS

[1]Institute of Laser Physics SB RAS, 15B Lavrentyev Avenue, Novosibirsk 630090, Russia
[2]Novosibirsk State University, 1 Pirogov Street, Novosibirsk 630090, Russia
[3]Institute of Electronics BAS, 72 Tsarigradsko Chaussee, Sofia 1784, Bulgaria
[4]Faculty of Physics, Sofia University "St. Kliment Ohridski," 5 James Bourchier Boulevard, Sofia 1164, Bulgaria
[5]Novosibirsk State Technical University, 20 Karl Marks Avenue, Novosibirsk 630073, Russia

[a)]Author to whom correspondence should be addressed: brazhnikov@laser.nsc.ru

ABSTRACT

Level-crossing (LC) resonances in alkali-metal vapors are widely used for atomic magnetometry. One of the most simple and robust techniques involves a single circularly polarized light wave, while a transverse magnetic field ($\mathbf{B}_x \perp \mathbf{k}$) is scanned around zero to observe the subnatural-linewidth resonance of electromagnetically induced transparency (EIT) in the light wave transmission. This technique allows miniaturization of the magnetic field sensor to a great extent, maintaining high sensitivity of measurements. To obtain a high quality factor of the LC resonance and, therefore, high performance of the sensor, either a high temperature (>120 °C) or an extended volume of the vapor cell ($V \gg 1$ cm^3) is usually required. Here, we propose a slight modification to the commonly used configuration, which can provide high-quality LC resonances in small ($\ll 1$ cm^3) vapor cells at a relatively low temperature of 60 °C or less. The modification consists in adding the second (pump) counterpropagating light wave with opposite circular polarization ($\sigma^+\sigma^-$ configuration). In our experiments, the waves excite the D_1-line ground-state level $F_g = 4$ in cesium atoms in the presence of a buffer gas (Ne, 130 Torr). In the proposed scheme, a subnatural-linewidth electromagnetically induced absorption (EIA) resonance is observed. We compare parameters of the EIA resonance with those obtained in the single-wave scheme to show benefits of using the proposed $\sigma^+\sigma^-$ configuration. The results have good prospects for developing a low-power miniaturized atomic magnetometer with a wide operating range.

Starting from the experiments of Wilhelm Hanle and his contemporaries, the level-crossing (LC) phenomenon in resonant atomic vapors has played a crucial role in the development of quantum mechanics[1,2] (see also a review in Ref. 3). The zero-field LC resonances are nowadays often studied as a change in the light wave intensity transmitted through a resonant medium when an ambient magnetic field is scanned. The level crossing in an atomic ground state—the ground-state Hanle effect (GSHE)—can provide much narrower magneto-optical resonances than the excited-state Hanle effect, especially if a buffer gas or an antirelaxation coating of the vapor cell walls is used.[4,5]

There is a large variety of laser spectroscopy methods that can be applied for magnetic field measurements.[6] The GSHE-based technique does not usually claim a record sensitivity as, for instance, some types of laboratory atomic magnetometers (AMs) based on registration of magneto-optical rotation under the spin-exchange relaxation-free (SERF) regime;[7–9] nevertheless, it remains a simple and robust technique, reaching a subpicotesla sensitivity. The method can be used for scalar,[4,5,10] two-axis,[11–14] or full three-axis (vector) measurements,[14–16] and the sensor can be significantly miniaturized.[10,17–19] Moreover, the crosstalk effects[20] occurring in a multi-channel mode of operation are relatively small in the Hanle magnetometers compared to some other types of AMs where an rf field is used. Therefore, the Hanle magnetometers are attractive for a wide range of applications, including biology and medicine.[17–19]

The simplest GSHE-based magnetic field sensor usually utilizes a single circularly polarized light wave (e.g., see Ref. 10). The wave

produces a macroscopic vector magnetization in the atomic ground state, following the σ optical transitions and the optical pumping process.[21] To observe the resonance, a transverse magnetic field ($\mathbf{B}_x \perp \mathbf{k}$ with $\mathbf{k}$ being the wave vector) is scanned around zero, and a light wave transmission through a vapor cell is registered. In this configuration, the so-called electromagnetically induced transparency (EIT) is usually observed.

Here, we describe a possibility how this standard configuration can be modified to obtain a significant improvement in the LC resonance parameters. We focus on a low temperature regime ($\lesssim$60 °C) and on the use of a small vapor cell with an inner volume of $\approx$0.1 cm^3. Such requirements are nowadays important for many applications where heat release, power consumption, and compactness of a sensor play a crucial role. We propose to use a cesium vapor rather than rubidium, potassium, or sodium ones. This choice is dictated by the fact that, on the one hand, Cs has the highest saturated vapor pressure and, on the other hand, it has the strongest hyperfine splitting (hfs) in the ground state [$\approx$ 9.2 GHz, see inset in Fig. 1(a)]. The former means that the vapor cell can operate at a relatively low temperature. For instance, K sensors usually operate at temperatures much higher than 100 °C.[22] The large ground-state hfs of Cs means that the atomic quantum system, during its interaction with the light field, remains open even at a relatively high buffer gas pressure. In other words, owing to the spontaneous decay process, atoms can be accumulated on the non-resonant ground-state level $F_g = 3$, while the level $F_g = 4$ is being excited by the light field. For a long time, many authors considered the latter as a parasitic effect. Indeed, in the standard Hanle configurations, both with circularly or linearly polarized light waves, the "openness" leads to serious degradation of both the EIT and the electromagnetically induced absorption (EIA) properties.[23–26] In Ref. 27, the authors proposed to overcome this problem by using potassium vapors, because the K ground-state hfs equals $\approx$0.46 GHz, which is smaller than the Doppler width of $\approx$0.77 GHz at 300 K. Consequently, the quantum system in this case is not open, i.e., both ground-state levels efficiently interact with the light field. The authors reported observation of a EIT resonance contrast up to 65% for a 50 mm long buffered K vapor cell at a linewidth of 13 mG, while under similar conditions, the resonance contrast in Cs vapors was $\approx$1%. However, potassium vapors require either a high temperature or an extended length of the cell to obtain a desirable degree of light field absorption. A similar reasoning can be applied to the sodium vapors.

The second (pump) light wave can be added to improve significantly the parameters of GSHE resonances.[28] An example of such an idea was verified in experiments with Rb[29] and Cs[30] buffer-gas vapor cells of $\sim$1 cm dimensions. Two counterpropagating waves with orthogonal linear polarizations were used (lin $\perp$ lin configuration), leading to observation of an EIA-type LC resonance in the probe wave transmission. A unique feature of the lin $\perp$ lin configuration is that the openness plays an essentially positive role for achieving high contrast of the resonances. In particular, in the case of Cs, a resonance contrast as high as 75% was achieved.

Unfortunately, the lin $\perp$ lin configuration is highly sensitive to a spectral resolution of the excited-state hfs levels.[30] Therefore, it cannot be employed for miniaturized vapor cells where narrow light beams and a relatively high buffer gas pressure are required. In addition, the configuration exhibits a shift effect,[31] which can affect deeply the magnetic field measurements. Here, we examine a configuration composed of a counterpropagating pump and probe beams with opposite circular polarizations [$\sigma^+\sigma^-$, see Fig. 1(a)]. It should be noted that similar configurations have already brought relevant results for developing atomic clocks.[32–34] Also, the same light field geometry was studied in Ref. 35 in a cm-size K vapor cell with antirelaxation coating of the walls. In the present study, we show that a buffer-gas-filled Cs vapor cell can provide much better contrast-to-width ratio (CWR) of the LC resonance, while the cell volume can be as small as $\approx$0.1 cm^3, making the results to be interesting for real applications. The considered configuration keeps all advantages of the lin $\perp$ lin scheme, while it allows using a higher buffer gas pressure and does not exhibit the shift effect.[31] Also, we compare the obtained results with those registered in a standard Hanle scheme using a single light wave in the same vapor cell to show the benefits from using the $\sigma^+\sigma^-$ configuration.

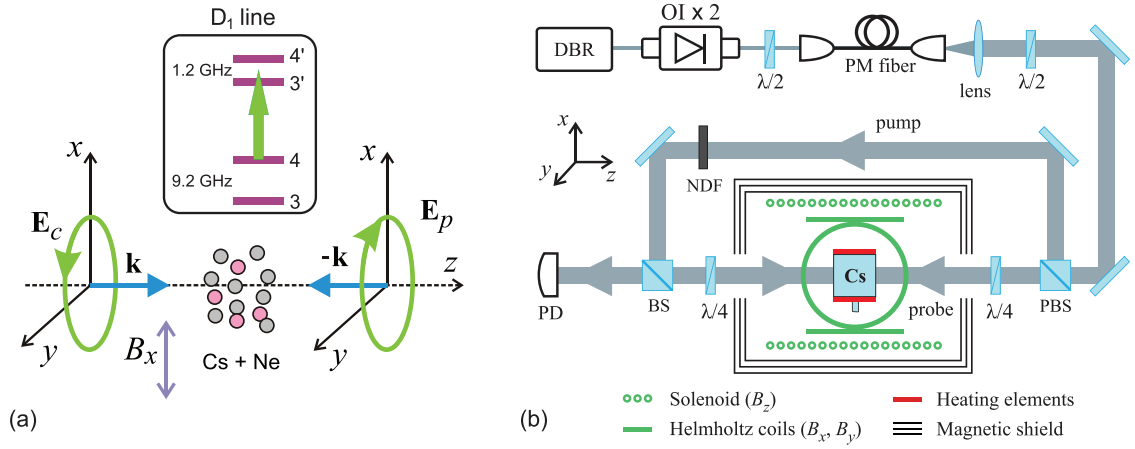

FIG. 1. (a) Light-field configuration with $\mathbf{E}_{c,p}$ being the circularly polarized control and probe waves, respectively. B_x field is scanned to observe the zero-field level-crossing resonance. (b) Experimental setup: DBR, distributed Bragg reflector diode laser; OI, optical Faraday insulator; PBS, polarizing beam splitter; BS, beam splitter; NDF, neutral density filter; PD, photodetector.

The experimental setup is shown in Fig. 1(b). We use a distributed Bragg reflector (DBR, Toptica LD-0895-0040) diode laser with a radiation wavelength of $\lambda = 894.6$ nm (Cs D_1 line) and a linewidth of $\leq$0.5 MHz. The laser output beam is passed through two Faraday optical isolators (OIs). Subsequently, it is sent to a polarization maintaining optical fiber. A half-wave plate ($\lambda/2$) before the fiber is used to adjust the linear polarization of the beam. A lens is placed after the fiber to collimate the beam. The combination of a half-wave plate placed after the fiber and a polarizing beam splitter (PBS) is used to redistribute the total light power between the pump and probe beams, which have orthogonal linear polarizations after the PBS. A beam splitter (BS) is used to direct the pump beam into the cell without affecting its polarization. The beam diameters in the cell ($1/e^2$) are $\approx$3 mm. A set of neutral density filters (NDFs) is used to tune the pump-wave power. Two quarter-wave plates ($\lambda/4$) are placed on both sides of the cell to produce the $\sigma^+\sigma^-$ configuration.

The cesium vapor cell is filled with a neon buffer gas ($\approx$120 Torr), and it has a cubic shape with an inner volume of $5 \times 5 \times 5 = 125$ mm^3. The cell is heated by an ac electric current (100 kHz) applied to special heating elements. The heating process does not have a visible effect on the LC resonances. A three-layer μ-metal magnetic shield is utilized to reduce the stray field to $\approx$0.1 mG in the cell area. The Doppler absorption profiles corresponding to the transitions $F_g = 4 \rightarrow F_e = 3$ and $F_g = 4 \rightarrow F_e = 4$ are significantly broadened due to buffer-gas collisions, and therefore, they are overlapped. The laser frequency is tuned manually to the center of the combined absorption profile. We use a solenoid to produce a longitudinal magnetic field ($\mathbf{B}_z||\mathbf{k}$) and two pairs of Helmholtz coils to produce transverse components ($\mathbf{B}_x$, $\mathbf{B}_y$).

An example of the GSHE resonance is shown in Fig. 2(a). The physical grounds for observing the high-contrast EIA-type LC resonances have many in common with those discussed in detail in Ref. 30 for a light-field configuration composed of linearly polarized waves. Here, for shortness, we just briefly describe them for the considered geometry. Figure 2(b) reflects a resonant interaction of the σ^+ polarized pump wave with the optical transitions $F_g = 4 \rightarrow F_e = 3, 4$ (green solid arrows). In the figure, magnetic (Zeeman) sub-levels of the excited state are not relevant for consideration and are not shown for simplicity. We assume the quantization axis z to be directed along the wave vectors [see Fig. 1(a)]. At $B_x = 0$ [Fig. 2(b), left], a significant part of the atoms is accumulated on the edge Zeeman sub-level $|F_g = 4, m_g = 4\rangle$, where they do not interact with the pump field due to the selection rules. This sub-level can be referred to as a trap state. In the present scheme, this state plays the same role in creation of the EIA resonance as the coherent-population-trapping (CPT) state in the linearly polarized waves.[30] The existence of the trap state leads to a small pump-wave absorption in the cell at $B_x = 0$. On the contrary, the counterpropagating σ^- probe wave (in the figure, it is shown, for shortness, as a single dashed blue arrow) experiences a strong interaction with the trap state that means a high probe-wave absorption [see the resonance curve in Fig. 2(a) at $B_x \approx 0$]. In Fig. 2(a), A denotes the resonance height, while B stands for the magnitude of the background transmission. P_c and P_p denote the pump (control) and the probe wave powers, respectively. Then, if $B_x \neq 0$ [Fig. 2(b), right], the Zeeman sub-levels are mixed by the transverse magnetic field, leading to the destruction of the trap state and thus to an increase in the pump-wave absorption. The latter, in turn, results in transferring most

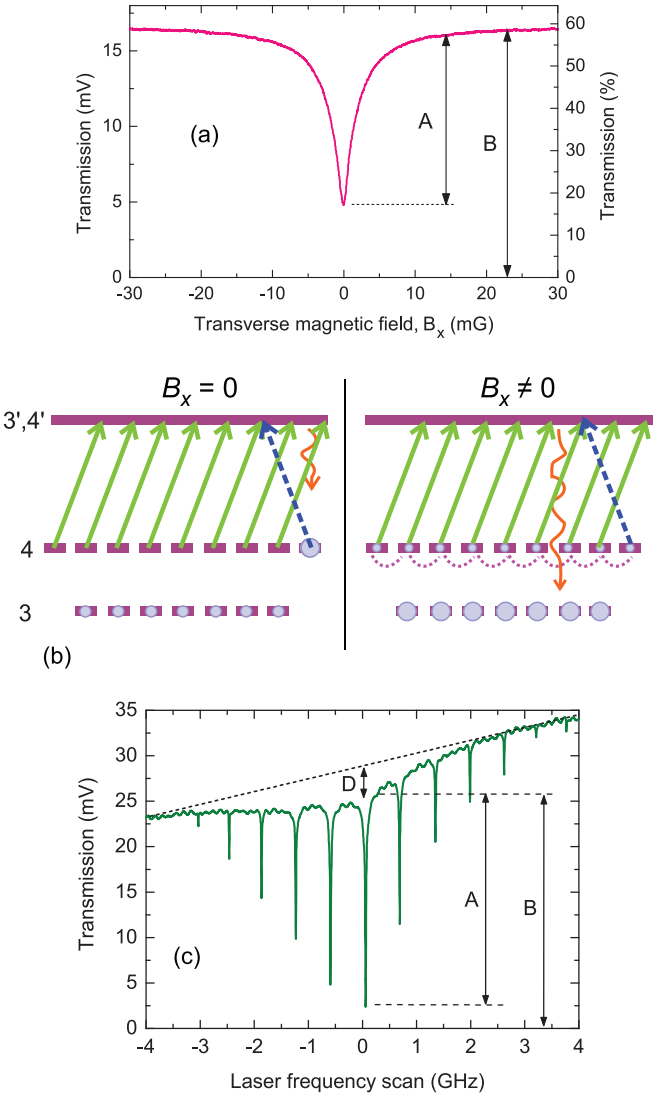

FIG. 2. (a) Level-crossing EIA resonance in the probe-wave transmission in mV at PD (left y axis) and normalized to the input probe wave power (right y axis). $P_c \approx 800\,\mu$W, $P_p \approx 5\,\mu$W, and $T_{cell} \approx 55\,^\circ$C. (b) Schematic presentation of atomic energy levels to explain observation of electromagnetically induced absorption resonance in the probe wave transmission (see details in the text). (c) Probe-wave transmission vs the laser frequency scan around the transitions $F_g = 4 \rightarrow F_e = 3, 4$ with simultaneous scan of the transverse magnetic field around zero as in (a). The frequencies of the scans are: $f_{mag} = 15$ Hz, $f_{las} = 0.5$ Hz. $P_c \approx 5.13$ mW, $P_p \approx 5\,\mu$W, and $T_{cell} \approx 60\,^\circ$C. The dotted line represents the signal level without absorption in the cell. The central spike contrast ($A/B \times 100\%$) is $\approx$92%.

atoms to the non-resonant ground-state level $F_g = 3$ via the optical pumping process (orange wavy arrow). Being on this level, the atoms do not scatter both the pump and the probe light waves [see the wings of the resonance curve in Fig. 2(a)]. This is how the EIA resonance is created in the $\sigma^+\sigma^-$ configuration.

Increasing the buffer gas pressure implies increase in the time of light-atom interaction. It leads, on the one hand, to a decrease in the

resonance linewidth and, on the other hand, to an increase in the efficiency of all the optical pumping processes mentioned above and depicted in Fig. 2(b). Namely, increasing the pressure causes an increase in both the degree of atomic spin polarization at $B_x = 0$ and in the number of atoms transferred to the non-resonant level $F_g = 3$ at $B_x \neq 0$. The described mechanism yields high-contrast narrow-linewidth LC resonances, hence the necessity of spectral resolution of the ground-state levels.

The plot in Fig. 2(c) demonstrates the probe-wave transmission vs the laser frequency scan around the transitions $F_g = 4 \rightarrow F_e = 3, 4$, while simultaneously scanning B_x around zero. As seen, the EIA LC resonances can have a very high contrast with respect to both the Doppler absorption profile (D) and the background transmission (B). This curve can be compared, for instance, with that obtained by Gozzini *et al.* for potassium vapors.[35] The comparison reveals a much higher contrast and CWR in the case of Cs vapors. In the current work, we focus on measuring the full width at half maximum (FWHM) of the resonance, its contrast defined as $C = (A/B) \times 100\%$ (see Fig. 2), and the contrast-to-width ratio (C/ FWHM). The latter is especially important for applications in magnetometry.

Figure 3 reveals the influence of the pump-wave intensity ($I_c = 4P_c/\pi d^2$) on the resonance parameters. The power broadening of the resonance is shown in Fig. 3(a). The zero power limit gives FWHM ≈0.6 mG (60 nT). The linewidth dependence does not show a significant difference between the regimes with $T_{\text{cell}} = 45\,^{\circ}\text{C}$ and $50\,^{\circ}\text{C}$. However, further increase in the temperature results in additional broadening, because the medium acquires a large optical density. The temperature increase, on the contrary, helps to observe an extremely high contrast of the resonance, reaching ≈99% [see Fig. 3(b)]. The competition between the linewidth and the contrast dependencies leads to the formation of an extremum in the contrast-to-width ratio [Fig. 3(c)]. This extremum shows that the optimal pump-wave intensity is not high (≈ 0.7 mW/cm^2). We should note that the observed CWR ≈45%/mG is relatively high, especially taking into account the cell size. For instance, in Ref. 27, the authors measured a CWR of the EIT resonance of ≈65/13 = 5%/mG in a 5 cm long K buffer-gas cell. In Ref. 36, the authors reported observation of an EIA LC resonance as narrow as 0.55 mG in a 5 cm long Rb vapor cell with antirelaxation coating. In spite of the small linewidth, a contrast of only 0.5% was achieved, yielding CWR ≈0.9%/mG. This parameter, however, can be crucial for achieving high sensitivity of a magnetic field sensor, since the sensitivity can be written in a general form as: $\delta B \approx \text{FWHM}/(\gamma \cdot \text{SNR})$ with γ being the gyromagnetic ratio and SNR being the signal-to-noise ratio. In our case, SNR is proportional to the resonance contrast.

Figure 4 demonstrates the benefits of using the $\sigma^+\sigma^-$ light-field configuration rather than the standard Hanle scheme where only one circularly polarized wave is used. In the latter case, an EIT resonance is observed. To compare the two configurations, we used the same setup as in Fig. 1, but with the pump wave switched off. As seen, the EIA resonance contrast demonstrates a fivefold increase with respect to the EIT one.

For applications in magnetometry, it is important that the linewidth of a magneto-optical resonance has a linear sensitivity to variations in the magnetic field. Obviously, a constant component B'_x of an ambient field, if presented in the cell, will lead to just a shift of the resonance that can be measured. Figure 5(a) shows that the other two components provide a truly linear broadening of the resonance. At the same time, as seen from Fig. 5(b), a static B_y field can significantly degrade the resonance contrast, because it mixes the Zeeman sublevels [see Fig. 2(b)]. Therefore, magnetic field measurements should be performed under a shielded environment[10] or by using additional compensation coils.[37] It is worth noting that these coils can be used for the realization of full three-axis (vector) measurements. In particular, a standard synchronous detection technique can be involved for obtaining a dispersion-like LC resonance (an error signal). This technique, in addition, helps to suppress the low-frequency noise, resulting to the better signal-to-noise ratio.[10] The scanning B_x field can be tuned

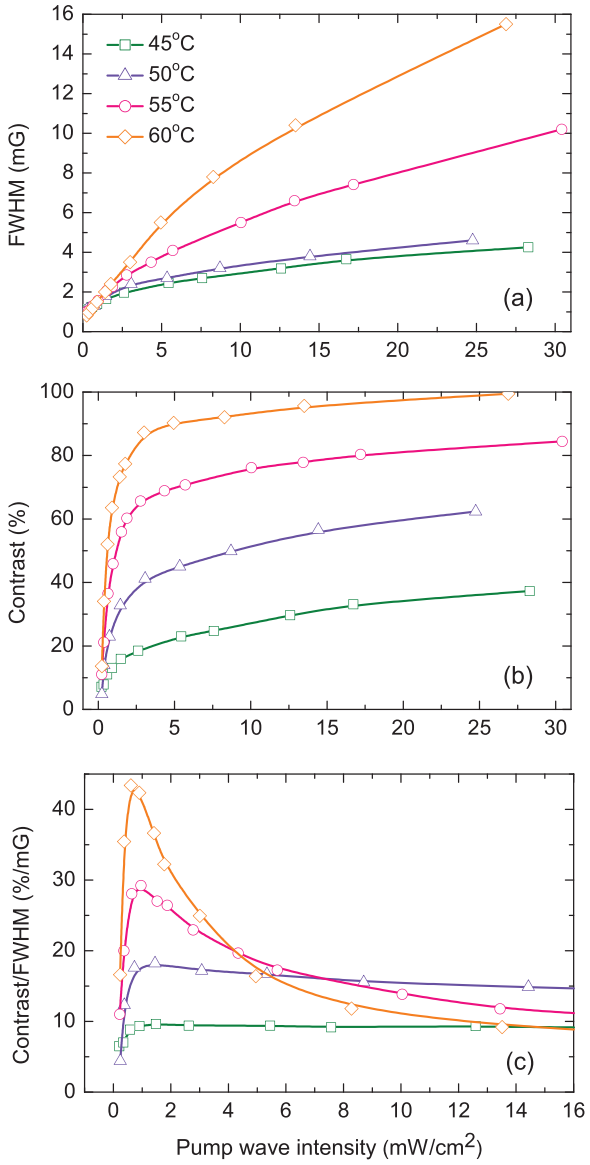

FIG. 3. Properties of the level-crossing EIA resonance vs the pump-wave intensity: (a) linewidth, (b) contrast, and (c) contrast-to-width ratio. The results are obtained for different cell temperatures. $P_p \approx 5\ \mu$W.

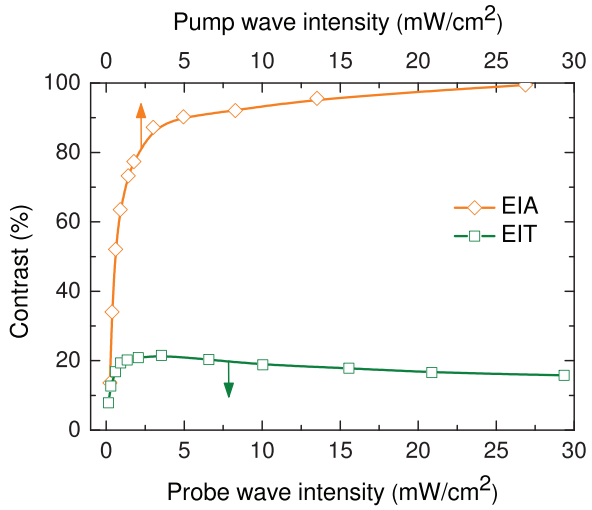

FIG. 4. Comparison of the contrast of the EIA resonance in the $\sigma^+\sigma^-$ configuration ($P_p \approx 5\ \mu$W) with the contrast of the EIT resonance in the standard Hanle configuration. $T_{cell} = 60\,^\circ$C.

to the center of the error signal, yielding information on the B'_x component of the ambient field. The other two compensation coils can be used to maximize the slope of the signal. The maximized slope means that the resonance has a maximum amplitude and a minimum linewidth, i.e., the ambient components B'_y, B'_z are compensated. They can be figured out from electric currents of the coils. It is important that such a 3D technique can be exploited under an unshielded environment and does not have any dead zone of measurements.

In conclusion, we reported a substantial improvement of the standard Hanle configuration for observing level-crossing resonances in buffered vapor cells. The proposed scheme implies using the additional pump wave, having the opposite circular polarization ($\sigma^+\sigma^-$ scheme). In contrast to our previous study with linearly polarized counterpropagating waves (lin $\perp$ lin scheme),[29,30] the current configuration has several crucial advantages. First, it allows applying much higher buffer gas pressure, meaning that miniature vapor cells ($V \ll 1$ cm) can be utilized. Second, it does not exhibit a parasitic shift effect[31] that can influence the magnetic field measurements. These peculiarities make the $\sigma^+\sigma^-$ scheme much more attractive for applications in atomic magnetometry than the lin $\perp$ lin one. Furthermore, by comparing our results with those observed in the standard single-beam scheme in the same vapor cell, we have revealed the fivefold improvement in the resonance contrast. Moreover, all the experiments have been carried out at relatively low temperature of the vapors (45–60 °C), meaning a low power consumption for heating the cell. Despite the addition of the second light wave, a magnetic field sensor can still be miniaturized by tight integration of optical components into a sensor head as it was demonstrated, for instance, by Knappe *et al.* for a microfabricated spectrometer.[38] Perhaps, an easier way is to use two independent light beams injected into the cell by optical fibers.[39,40] Another possibility is to use a co-propagating $\sigma^+\sigma^-$ configuration. The latter, however, needs to be studied separately.

To summarize, the results can be applied for developing a miniaturized low-power magnetic field sensor with high sensitivity. Such a

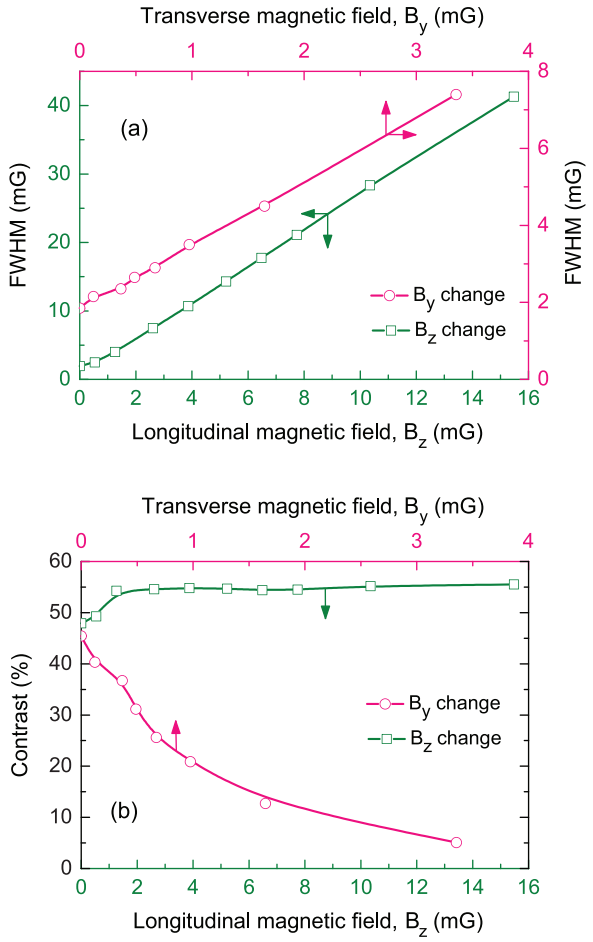

FIG. 5. EIA resonance linewidth (a) and contrast (b) as functions of the B_y and B_z components of an ambient magnetic field. $P_c \approx 265\ \mu$W, $P_p \approx 5\ \mu$W, and $T_{cell} = 50\,^\circ$C.

sensor can be used both in shielded and unshielded environments. Although an additional study is required to characterize in full the parameters of the sensor, nevertheless, by comparing our results with those presented in other papers,[10,37] we anticipate the potential sensitivity to be well below 100 fT/Hz$^{1/2}$.

The authors acknowledge support from the Russian Foundation for Basic Research (No. 20-52-18004) and the Bulgarian National Science Fund (No. KP-06-Russia/11) in the framework of a joint research project. We also thank the Russian Science Foundation (No. 17-72-20089). I. S. Mesenzova has also been supported by the Ministry of Science and Higher Education of the Russian Federation (Presidential Scholarship No. SP-269.2021.3).

DATA AVAILABILITY

The data that support the findings of this study are available from the corresponding author upon reasonable request.

REFERENCES

[1]W. Hanle, Z. Phys. **30**, 93 (1924).
[2]G. Breit, Rev. Mod. Phys. **5**, 91 (1933).
[3]W. Gawlik, D. Gawlik, and H. Walther, "The Hanle effect and atomic physics," in *The Hanle Effect and Level-Crossing Spectroscopy*, edited by G. Moruzzi and F. Strumia (Springer, New York, 1991).
[4]E. B. Aleksandrov, A. M. Bonch-Bruevich, and V. A. Khodovoi, Opt. Spectrosc. **23**, 151 (1967).
[5]J. Dupont-Roc, S. Haroche, and C. Cohen-Tannoudji, Phys. Lett. A **28**, 638 (1969).
[6]D. Budker, W. Gawlik, D. F. Kimball, S. M. Rochester, V. V. Yashchuk, and A. Weis, Rev. Mod. Phys. **74**, 1153 (2002).
[7]J. C. Allred, R. N. Lyman, T. W. Kornack, and M. V. Romalis, Phys. Rev. Lett. **89**, 130801 (2002).
[8]I. K. Kominis, T. W. Kornack, J. C. Allred, and M. V. Romalis, Nature **422**, 596 (2003).
[9]S. J. Seltzer and M. V. Romalis, Appl. Phys. Lett. **85**, 4804 (2004).
[10]V. Shah, S. Knappe, P. D. D. Schwindt, and J. Kitching, Nat. Photonics **1**, 649 (2007).
[11]A. Papoyan, S. Shmavonyan, A. Khanbekyan, K. Khanbekyan, C. Marinelli, and E. Mariotti, Appl. Opt. **55**, 892 (2016).
[12]R. S. Grewal and M. Pattabiraman, Eur. Phys. J. D **70**, 219 (2016).
[13]H. Azizbekyan, S. Shmavonyan, A. Khanbekyan, M. Movsisyan, and A. Papoyan, Opt. Eng. **56**, 074104 (2017).
[14]G. L. Gal, G. Lieb, F. Beato, T. Jager, H. Gilles, and A. Palacios-Laloy, Phys. Rev. Appl. **12**, 064010 (2019).
[15]E. Alipieva, S. V. Gateva, and E. Taskova, IEEE Trans. Instrum. Meas. **54**, 738 (2005).
[16]R. Behera and S. Pradhan, J. Phys. B **53**, 205001 (2020).
[17]O. Alem, T. H. Sander, R. Mhaskar, J. LeBlanc, H. Eswaran, U. Steinhoff, Y. Okada, J. Kitching, L. Trahms, and S. Knappe, Phys. Med. Biol. **60**, 4797 (2015).
[18]J. Osborne, J. Orton, O. Alem, and V. Shah, Proc. SPIE **10548**, 105481G (2018).
[19]E. J. Pratt *et al.*, Proc. SPIE **11700**, 1170032 (2021).
[20]K. Kim, S. Begus, H. Xia, S.-K. Lee, V. Jazbinsek, Z. Trontelj, and M. V. Romalis, NeuroImage **89**, 143 (2014).
[21]W. Happer, Rev. Mod. Phys. **44**, 169 (1972).
[22]H. Xia, B. A. Baranga, D. Hoffman, and M. V. Romalis, Appl. Phys. Lett. **89**, 211104 (2006).
[23]A. V. Papoyan, M. Auzinsh, and K. Bergmann, Eur. Phys. J. D **21**, 63 (2002).
[24]A. S. Zibrov and A. B. Matsko, JETP Lett. **82**, 472 (2005).
[25]M. Auzinsh, A. Berzins, R. Ferber, F. Gahbauer, L. Kalvans, A. Mozers, and D. Opalevs, Phys. Rev. A **85**, 033418 (2012).
[26]R. S. Grewal and M. Pattabiraman, J. Phys. B **48**, 085501 (2015).
[27]S. Gozzini, S. Cartaleva, A. Lucchesini, C. Marinelli, L. Marmugi, D. Slavov, and T. Karaulanov, Eur. Phys. J. D **53**, 153 (2009).
[28]D. V. Brazhnikov, A. V. Taichenachev, A. M. Tumaikin, and V. I. Yudin, Laser Phys. Lett. **11**, 125702 (2014).
[29]D. V. Brazhnikov, S. M. Ignatovich, V. I. Vishnyakov, M. N. Skvortsov, C. Andreeva, V. M. Entin, and I. I. Ryabtsev, Laser Phys. Lett. **15**, 025701 (2018).
[30]D. V. Brazhnikov, S. M. Ignatovich, A. S. Novokreshchenov, and M. N. Skvortsov, J. Phys. B **52**, 215002 (2019).
[31]D. Brazhnikov, S. Ignatovich, I. Mesenzova, A. Novokreshchenov, and A. Goncharov, Opt. Lett. **45**, 3309 (2020).
[32]A. V. Taichenachev, V. I. Yudin, V. L. Velichansky, S. V. Kargapoltsev, R. Wynands, J. Kitching, and L. Hollberg, JETP Lett. **80**, 236 (2004).
[33]X. Liu, V. I. Yudin, A. V. Taichenachev, J. Kitching, and E. A. Donley, Appl. Phys. Lett. **111**, 224102 (2017).
[34]D. Brazhnikov, S. Ignatovich, V. Vishnyakov, R. Boudot, and M. Skvortsov, Opt. Express **27**, 36034 (2019).
[35]S. Gozzini, A. Fioretti, A. Lucchesini, L. Marmugi, C. Marinelli, S. Tsvetkov, S. Gateva, and S. Cartaleva, Opt. Lett. **42**, 2930 (2017).
[36]H. J. Kim and H. S. Moon, Opt. Express **19**, 168 (2011).
[37]V. K. Shah and R. T. Wakai, Phys. Med. Biol. **58**, 8153 (2013).
[38]S. A. Knappe, H. G. Robinson, and L. Hollberg, Opt. Express **15**, 6293 (2007).
[39]J. Preusser, V. Gerginov, S. Knappe, and J. Kitching, in *Proceedings of the IEEE Sensors Conference* (IEEE, 2008), p. 344.
[40]T. H. Sander, J. Preusser, R. Mhaskar, J. Kitching, L. Trahms, and S. Knappe, Biomed. Opt. Express **3**, 981 (2012).